Reduction of the pulse spike-cut error in Fourier-deconvolved lidar profiles

D. V. Stoyanov, L. L. Gurdev, and T. N. Dreischuh

A simple approach is analyzed and applied to the National Oceanic and Atmospheric Administration (NOAA) Doppler lidar data to reduce the error in Fourier-deconvolved lidar profiles that is caused by spike-cut uncertainty in the laser pulse shape, i.e., uncertainty of the type of not well-recorded (cut, missed) pulse spikes. Such a type of uncertainty is intrinsic to the case of TE (TEA) CO_2 laser transmitters. This approach requires only an estimate of the spike area to be known. The result from the analytical estimation of error reduction is in agreement with the results from the NOAA lidar data processing and from computer simulation.

1. Description of the Problem

The lidar resolution is usually of the order of the sensing laser pulse length.[1] So the long-pulse [e.g., TE (TEA) CO_2] coherent Doppler lidars ensure satisfactory accuracy in the measurement of Doppler velocities but they have a too low spatial resolution (~200–500 m) because of which the information about small-scale atmospheric inhomogeneities is lost.[2] In general, the lidar return signal $F(t)$ at moment t after pulse emission is given by the convolution

$$F(t) = \int_{-\infty}^{\infty} S(t - 2z'/c)\Phi(z')\mathrm{d}z' \qquad (1)$$

of the pulse shape $S(\vartheta)$ and the maximum-resolved (short-pulse) lidar profile $\Phi(z)$. In Eq. (1), c is the speed of light and z' is the coordinate along the line of sight; $S(\vartheta) = P(\vartheta)/P_p$, where $P(\vartheta)$ is the pulse power shape and P_p is its peak value. Here and everywhere below moment t corresponds to the longitudinal coordinate $z \equiv ct/2 (t \equiv 2z/c)$. A way to improve the lidar resolution is to solve Eq. (1) with respect to $\Phi(z)$. In this way one can identify the small-scale (e.g., aerosol) inhomogeneities in the atmosphere and thus improve the performance of the long-pulse lidars. Therefore we have developed[3,4] deconvolution techniques to invert Eq. (1) when the pulse shape $S(\vartheta)$ is known without any uncertainty. These techniques, based on Fourier transformation or a Volterra integral equation or a recurrence relation, ensure good quality for retrieval of the fine atmospheric structure in the absence and presence of noise. The Fourier-deconvolution algorithm is based on the expression[4]

$$\Phi(t) = (\pi c)^{-1} \int_{-\infty}^{\infty} \Im_d(\omega)\tilde{F}(\omega)\exp(-j\omega t)\mathrm{d}\omega, \qquad (2)$$

where $\Im_d(\omega) = [\tilde{S}(\omega)]^{-1}$ is the Fourier-deconvolving inverse filter, and the quantity $\tilde{X}(\omega) = \int_{-\infty}^{\infty} X(\vartheta)\exp(j\omega\vartheta)\mathrm{d}\vartheta$ is the Fourier transform of a function $X(\vartheta)$ of some time variable ϑ; j is imaginary unity. Because of various factors the shape $S(\vartheta)$ might be determined with some regular (deterministic) or random uncertainties that would lead to errors in the determination of $\Phi(z)$. The behavior of the Fourier-deconvolution error $\delta_\Phi(t)$ caused by pulse-shape uncertainties has been investigated in detail in Refs. 5 and 6 from which the following general expression was obtained:

$$\delta_\Phi(t) = \Phi_r(t) - \Phi(t) = -(2\pi)^{-1} \int_{-\infty}^{\infty} \tilde{\Phi}(\omega)\Im_e(\omega)\exp(-j\omega t)\mathrm{d}\omega. \qquad (3)$$

In Eq. (3) $\Im_e(\omega) = \tilde{f}(\omega)[\tilde{S}(\omega) + \tilde{f}(\omega)]^{-1}$, $\Phi_r(t)$ is the lidar profile restored with use of the measured pulse shape $S_m(\vartheta) = S(\vartheta) + f(\vartheta)$ considered as a sum of the true pulse shape $S(\vartheta)$ and the uncertainty $f(\vartheta)$ in its measurement; $\tilde{\Phi}(\omega)$ and $\tilde{f}(\omega)$ are Fourier transforms

The authors are with the Institute of Electronics, Bulgarian Academy of Sciences, 72 Tzarigradsko shosse Boulevard, Sofia BG-1784, Bulgaria.

Received 9 June 1995; revised manuscript received 29 February 1996.

0003-6935/96/244798-05$10.00/0

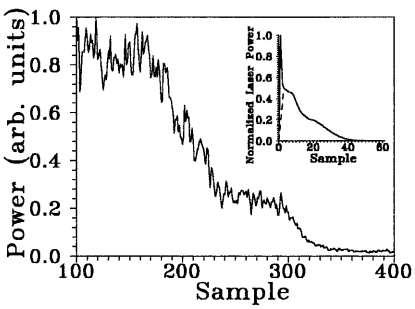

Fig. 1. Lidar power profile $F(t)$ averaged over 32 laser shots (NOAA data) and model of a laser pulse shape as a function of sample number (inset). The dashed curve in the inset divides the cut (not recorded) pulse spike from the remaining (recorded) pulse tail.

of $\Phi(t)$ and $f(\vartheta)$, respectively. A typical case of a fast-varying short-range uncertainty is the cut of a pulse spike, which is essential for the TE (TEA) CO_2 lidars having numerous advantages in direct or heterodyne modes of detection.[7] The model of a TE (TEA) CO_2 laser pulse shape is shown in Fig. 1. It consists of an initial spike followed by a long tail. The spike is often not well recorded[8] (it is cut) because of a large sampling interval. In this case one can represent the true pulse shape $S(\vartheta)$ as the sum $S(\vartheta) = f_R(\vartheta) + f_S(\vartheta)$ of the spike $f_S(\vartheta)$ and the remaining pulse $f_R(\vartheta)$, whose Fourier transforms are $\tilde{f}_S(\omega)$ and $\tilde{f}_R(\omega)$, respectively. Obviously, the spike cut (omission of the spike) can be considered as a negative sign uncertainty $f(\vartheta) = -f_S(\vartheta)$ so that $S_m(\vartheta) = S(\vartheta) + f(\vartheta) = f_R(\vartheta)$. Then one can perform the deconvolution only with the use of $f_R(\vartheta)$ $[\tilde{f}_R(\omega)]$ since in Eq. (2) we already have $\Im_d(\omega) = \Im_{d1}(\omega) = [f_R(\omega)]^{-1}$, and the corresponding error will be

$$\delta_\Phi(t) = \delta_{\Phi 1}(t) = (2\pi)^{-1} \int_{-\infty}^{\infty} \tilde{\delta}_{\Phi 1}(\omega) \exp(-j\omega t) \mathrm{d}\omega, \quad (4)$$

where $\tilde{\delta}_{\Phi 1}(\omega) = -\tilde{\Phi}(\omega)\Im_{e1}(\omega)$ is the Fourier transform of $\delta_{\Phi 1}(t)$ and $\Im_e(\omega) = \Im_{e1}(\omega) = -\tilde{f}_S(\omega)/\tilde{f}_R(\omega)$. As shown in Refs. 5 and 6, the spike-cut error $\delta_{\Phi 1}(t)$ (caused by the cut of the spike) consists in a shift up as a whole of the restored lidar profile (with respect to the true one) as well as of distortions in the spectrum of the retrieved inhomogeneities.

Our purpose in this paper is to describe and to discuss a simple way to reduce the Fourier-deconvolution error by use of an appropriate approximation $\tilde{f}_{Sa}(\omega)$ instead of the unknown precise spike spectrum $\tilde{f}_S(\omega)$. Despite the discrete numerical character of the actual calculations, in our analysis we used the convenient Fourier integral technique that allowed us to obtain useful analytical estimates of the deconvolution error and the error reduction ratio, both of which are valid for discrete data processing.

2. Error Reduction

A way to avoid or reduce the spike-cut error is to increase the sampling rate, but this approach leads to hardware problems such as a higher data rate and lower dynamic range. Another way to avoid the above-mentioned difficulties would be to compensate the absence in the $\Im_d(\omega)$ spectrum $\tilde{f}_S(\omega)$ by some approximation $\tilde{f}_{Sa}(\omega)$ of it. Then the deconvolving filter $\Im_d(\omega) = \Im_{d2}(\omega) = [\tilde{f}_R(\omega) + \tilde{f}_{Sa}(\omega)]^{-1}$, which is much more like the true filter $\Im_d(\omega) = [\tilde{f}_R(\omega) + \tilde{f}_S(\omega)]^{-1} = [\tilde{S}(\omega)]^{-1}$, must lead to a reduction of the deconvolution error. The function $\Im_{d2}(\omega)$ can be represented in the form $\Im_{d2}(\omega) = [\tilde{S}(\omega) + \tilde{f}_n(\omega)]^{-1}$, where $\tilde{f}_n(\omega) = \tilde{f}_{Sa}(\omega) - \tilde{f}_S(\omega)$ is interpreted as the spectrum that corresponds to some new uncertainty $f(\vartheta) = f_n(\vartheta)$. In this case the comparison of Eq. (3), for $\tilde{f}(\omega) = \tilde{f}_n(\omega)$, with Eq. (4) leads to the following expression of the deconvolution error:

$$\delta_\Phi(t) = \delta_{\Phi 2}(t) = (2\pi)^{-1} \int_{-\infty}^{\infty} \delta_{\Phi 1}(\omega)\chi(\omega)\exp(-j\omega t)\mathrm{d}\omega, \quad (5)$$

where the reduction factor $\chi(\omega) = -\{[\tilde{f}_n(\omega)/\tilde{f}_S(\omega)]\tilde{f}_R(\omega)\}/[\tilde{S}(\omega) + \tilde{f}_n(\omega)]$. An approximation of the spike spectrum

$$\tilde{f}_S(\omega) = \int_{-\infty}^{\infty} f_S(\vartheta)\exp(j\omega\vartheta)\mathrm{d}\vartheta \quad (6a)$$

follows from the short spike duration that is of the order of the sampling interval Δt. Then the exponential integrand factor $[\exp(j\omega\vartheta)]$ in Eq. (6a) is a slowly varying function compared with $f_S(\vartheta)$ even at frequencies ω of the order of the Nyquist frequency $\omega_N = \pi/\Delta t$. Instead of Eq. (6a) this allows us to write

$$\tilde{f}_S(\omega) \approx \tilde{f}_{Sa}(\omega) = p_S \exp(j\omega t_m), \quad (6b)$$

where $p_S = \tilde{f}_S(0)$ is the spike area and t_m is the moment with respect to the spike beginning, at which the spike reaches its peak value of f_{Sm}. Since the spike duration is of the order of or less than the sampling interval Δt, the spectral width of $\tilde{f}_S(\omega)$ [as well as of $\tilde{f}_{Sa}(\omega)$] will be of the order of or larger than ω_N, which implies that it is many times as large as the calculation step $\Delta\omega$ in the frequency domain. Thus, although the spike is cut in the time domain, its spectrum $\tilde{f}_S(\omega)$ and the appropriate approximation $\tilde{f}_{Sa}(\omega)$ is well described in the frequency domain and contributes to error reduction.

To obtain an estimate of $\tilde{f}_{Sa}(\omega)$ to be used in the real calculations one should have some estimates $\hat{p}_S$ and $\hat{t}_m$ of p_S and t_m, respectively. The corresponding estimation errors are $\Delta = \hat{p}_S - p_S$ ($|\Delta| \ll p_S$) and $\Delta_m = \hat{t}_m - t_m$. The value of $\hat{t}_m = \Delta t$ may be considered as an estimate of t_m because the spike duration is of the order of the sampling interval. In this case we have $\Delta_m = \Delta t - t_m$. One can obtain estimates of p_S by the use of different techniques such as fast oscillograms or high-speed analog-to-digital converters. The relations between the concentrations of the gas components of the active laser medium can also be used to estimate the pulse-spike shape and p_S.[9] One can also use regression dependencies $p_S = g(f_{Sm})$ (of the spike area on the pulse maximum) that can, in principle, be determined separately and used thereafter for concrete lidar experiments to estimate p_S by mea-

suring f_{Sm} at each laser shot. Thus the actual approximation of $\tilde{f}_S(\omega)$ is

$$\tilde{f}_{Sa}(\omega) = (p_S + \Delta)\exp[j\omega(t_m + \Delta_m)] = \hat{p}_S \exp(j\omega\Delta t), \quad (6c)$$

and the expression of $\tilde{f}_n(\omega)$ acquires the form

$$\tilde{f}_n(\omega) = \exp[j\omega(t_m + \Delta_m)]\left(\Delta + \int d\vartheta f_S(\vartheta) \times \{1 - \exp[j\omega(\vartheta - t_m - \Delta_m)]\}\right). \quad (7a)$$

The integrand factor in brackets in Eq. (7a) is a slowly varying function compared with $f_S(\vartheta)$. Therefore when we perform the integration we can use the Taylor series expansion of this factor around the value of $\vartheta = t_m$. When only the first two terms of the expansion are used we obtain the following simplified expression of $\tilde{f}_n(\omega)$:

$$\tilde{f}_n(\omega) \approx \exp[j\omega(t_m + \Delta_m)](\Delta + p_S\{1 - [1 + j\omega \times (\bar{\vartheta} - t_m)]\exp(-j\omega\Delta_m)\}), \quad (7b)$$

where $\bar{\vartheta} = p_S^{-1} \int \vartheta f_S(\vartheta)d\vartheta$. An analysis of Eq. (5) shows that the essential integration area with respect to ω can be determined by some upper limit $\omega = \omega_l$ at which the spectrum $\tilde{\Phi}(\omega) = \tilde{\Phi}(\omega_l)$ is practically equal to zero. In this case even in the presence of restricted components of $\Phi(z)$, which are shorter than (but of the order of) the tail duration, we have $|\tilde{f}_R(\omega_l)| > |\tilde{f}_{Sa}(\omega_l)| = p_S$. Then in Eq. (5) we can approximately assume that [see approximations (6b) and (7b)] $\chi(\omega) \approx -\tilde{f}_n(\omega)/\tilde{f}_S(\omega) \approx -\tilde{f}_n(\omega)/\tilde{f}_{Sa}(\omega) = -\exp(j\omega\Delta_m)\{\Delta/p_S + 1 - [1 + j\omega(\bar{\vartheta} - t_m)]\exp(-j\omega\Delta_m)\}$. The last approximation of $\chi(\omega)$ allows us to transform the expression of the error given by Eq. (5) to the following explicit form:

$$\begin{aligned}\delta_{\Phi 2}(t) &\approx -[(1 + \Delta/p_S)\delta_{\Phi 1}(t - \Delta_m) - \delta_{\Phi 1}(t) + (\bar{\vartheta} - t_m)\delta'_{\Phi 1}(t)] \\ &\approx -(\Delta/p_S)\delta_{\Phi 1}(t) - \delta'_{\Phi 1}(t)[(\bar{\vartheta} - \Delta t) - (\Delta/p_S)\Delta_m],\end{aligned} \quad (8a)$$

where the prime denotes the first derivative. On the basis of the supposition that $\Delta/p_S \ll 1$ and $|\bar{\vartheta} - \Delta t| \sim |\Delta_m| < \Delta t$, approximation (8a) can be simplified to the form

$$\delta_{\Phi 2}(t) \approx -(\Delta/p_S)\delta_{\Phi 1}(t) - (\bar{\vartheta} - \Delta t)\delta'_{\Phi 1}(t). \quad (8b)$$

When $|\Delta/p_S| \ll 1$, the module of the first term on the right-hand side in approximations (8a) and (8b) is much less than $|\delta_{\Phi 1}|$. In addition, the module $|\delta'_{\Phi 1}(t)\|\bar{\vartheta} - \Delta t - (\Delta/p_S)\Delta_m|$ (or $|\delta'_{\Phi 1}(t)\|\bar{\vartheta} - \Delta t|$) of the second term in approximation (8a) [or approximation (8b)] is always small compared with the maxima of $|\delta_{\Phi 1}|$ when $|\bar{\vartheta} - \Delta t| \sim |\Delta_m| < \Delta t$, and Δt implies less than the characteristic period of varying $\Phi(t)$ and consequently $\delta_{\Phi 1}$ (see Ref. 6). So we can conclude that the compensation of the absent spike spectrum $\tilde{f}_S(\omega)$ by the approximation $\tilde{f}_{Sa}(\omega) = \hat{p}_S \exp(j\omega\Delta t)$ in the inverse Fourier-deconvolving filter $\Im_d(\omega)$ leads to a reduction of the deconvolution error range.

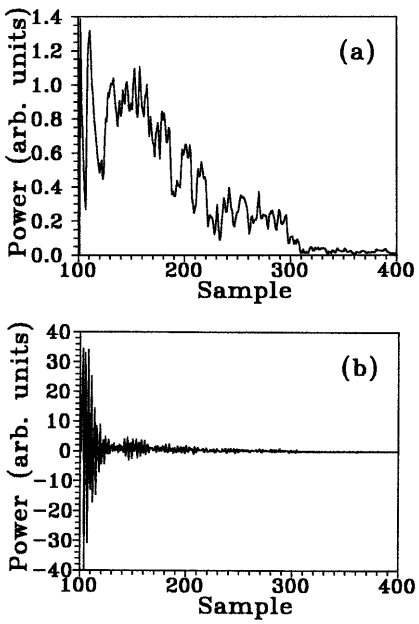

Fig. 2. Results of Fourier deconvolution of the lidar profile $F(t)$ in Fig. 1: (a) by use of the actual (the whole) pulse-shape spectrum and (b) without taking into account the unknown spectrum of the lost (cut) pulse spike.

3. Simulations and Real Data Processing

We have applied the above error-reduction procedure to a raw-data National Oceanic and Atmospheric Administration (NOAA) Doppler lidar power profile $F(t)$ that was obtained by averaging over 32 laser shots (Fig. 1). The averaging is intended for reduction of the speckle effects. In Fig. 1 and in the following figures the abscissa is given as samples, where a sample is assumed to be equal to 15 m corresponding to 0.1 μs. A laser pulse shape used in the simulations is represented in the inset of Fig. 1. It was constructed on the basis of the NOAA Doppler lidar data[8] to provide the pulse tail and an estimate of the pulse peak and on the assumption that the pulse is a gain-switched type. The Fourier-deconvolved lidar profile with the actual (the whole) pulse spectrum $\tilde{S}(\omega)$ is shown in Fig. 2(a). The effect of the spike cut on the deconvolved profile is shown in Fig. 2(b). As can be seen, the lidar information is destroyed because of the narrow bandwidth of the tail spectrum $\tilde{f}_R(\omega)$, which leads to a transformation of the high-frequency components (corresponding to the small-scale scattering inhomogeneities) of the lidar profile $F(t)$ into noise after deconvolution.

To consider the error reduction more precisely we simulated the restoration process without and with the addition of $\tilde{f}_{Sa}(\omega)$ to $f_R(\omega)$. The model of the lidar profile $\Phi(t)$ [see Fig. 3(a)] consists of a smooth component, a high-resolution component at near distances, and a triple-peak structure that can be used to introduce discontinuities at a relatively far range. We used the same sampling interval and pulse shape

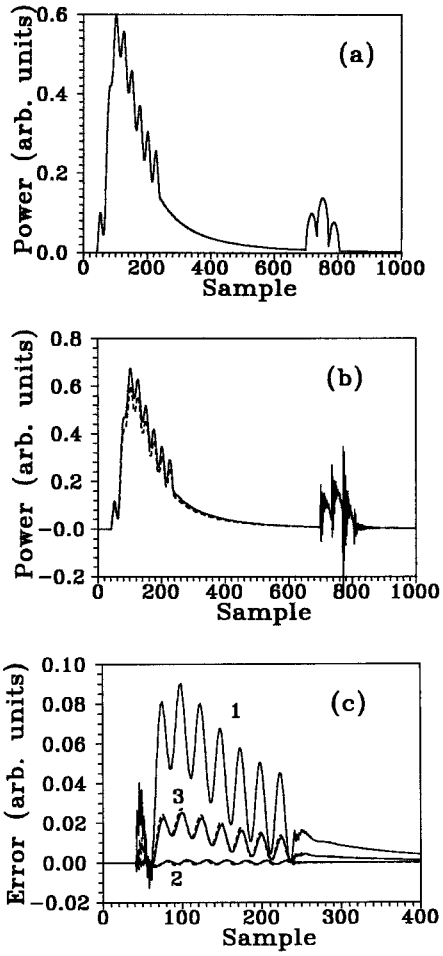

Fig. 3. (a) Model of the original short-pulse lidar profile $\Phi(t)$ used in the simulations; (b) the original profile (dashed curve) and the profile that was restored with the use of the pulse tail only; (c) restoration errors for the cases without spike spectrum compensation (curve 1) and with spike spectrum compensation (solid curves 2 and 3) at $\Delta = 0$ and $\Delta = -0.3p_S$, respectively. Dashed curves 2 and 3 represent the corresponding analytical dependencies [approximation (8b)].

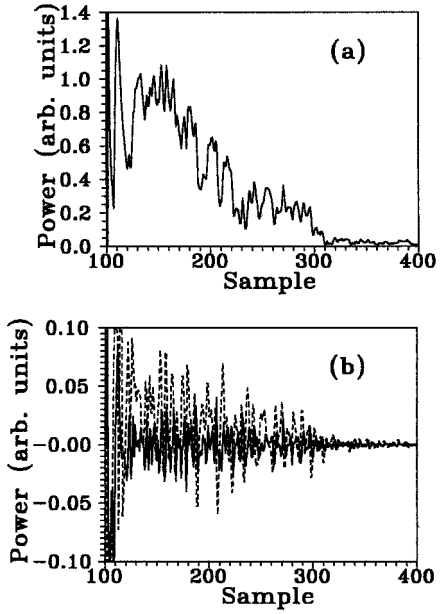

Fig. 4. (a) Result of Fourier deconvolution of the lidar profile $F(t)$ in Fig. 1 by spike spectrum compensation at $\Delta = 0$ and (b) computed errors in the deconvolution of the NOAA lidar profile given in Fig. 1 by use of spike spectrum compensation at $\Delta = 0$ (solid curve) and $\Delta = -0.3p_S$ (dashed curve). The errors were calculated with respect to the lidar profile that was restored by use of the true (whole) pulse spectrum.

as that described above. The deconvolved profile with the use of the pulse tail only (solid curve) is compared with the true short-pulse lidar profile (dashed curve) in Fig. 3(b). It can be seen that to disregard the unknown spike spectrum leads to a typical spike-cut deconvolution error (see Ref. 6). The profile $\Phi_r(t)$ restored by the use of $\tilde{f}_{Sa}(\omega)$ for compensation of $\tilde{f}_S(\omega)$ is not shown separately because it practically coincides with the initial profile [Fig. 3(a)] including the discontinuity region where the deconvolution without spike compensation leads to strong distortions. In Fig. 3(c) we have compared the restoration errors $\delta_{\Phi 1}$ and $\delta_{\Phi 2}$ for the cases, respectively, without and with spike spectrum compensation. One can see that the range of the latter error is essentially less than that of the first. It can also be seen that the behavior of the reduced error $\delta_{\Phi 2}$ for $\Delta = 0$ is described correctly by the analytical expression of approximation (8b), which is also represented graphically in Fig. 3(c). In the same figure we compared the reduced restoration error $\delta_{\Phi 2}(t)$ when $\Delta = -0.3p_S$ with the analytical dependence given by approximation (8b). Evidently there is good agreement between both dependencies. We also note that, even at $|\Delta/p_S| = 30\%$, the error $\delta_{\Phi 2}(t)$ is still too small compared with the error $\delta_{\Phi 1}(t)$. Therefore in many cases one can use estimates of $\hat{p}_S$ that were obtained by use of fast oscillograms or high-speed analog-to-digital converters. When regression curve $\hat{p}_S = g(f_{Sm})$ ensures a more accurate estimation of p_S (by the measurement of f_{Sm} at each laser shot), it provides better error reduction that is comparable with the case of $\Delta = 0$.

The Fourier-deconvolved (by spike spectrum compensation at $\Delta = 0$) NOAA lidar profile is shown in Fig. 4(a). One can see clear-cut inhomogeneities of the lidar profile including the cases of sharp increases of backscattered power. Because of a considerable reduction of the error the restored profile in Fig. 4(a) nearly coincides with the profile in Fig. 2(a) that was restored by use of the true pulse spectrum $\tilde{S}(\omega)$. The behavior of the retrieval error $\delta_{\Phi 2}$ [determined with respect to the profile $\Phi_r(t)$ restored by use of the true pulse spectrum $\tilde{S}(\omega)$] for $\Delta = 0$ and $\Delta = -0.3p_S$ is represented in Fig. 4(b). The results confirm the efficiency of the approach proposed and discussed here for reduction of the deconvolution error, which allows one to retrieve correctly the atmospheric inhomogeneities when they are sensed by long-pulse Doppler lidars.

4. Conclusion

Since a spike-cut uncertainty in the laser pulse shape may lead to unacceptable distortions of the Fourier-deconvolved lidar profiles, a simple approach has been proposed and analyzed to reduce these distortions, which is based on the use of approximation $\tilde{f}_{Sa}(\omega) = \hat{p}_S \exp(j\omega\Delta t)$ instead of the unknown true spike spectrum $\tilde{f}_S(\omega)$. The error-reduction efficiency has been demonstrated by computer simulations and processing of real NOAA Doppler lidar data. As an advantage, the error-reduction procedure does not require any additional hardware for the lidar system. The decrease of the spike-cut deconvolution error leads to an increase of the possibility to obtain lidar power profiles with high resolution. So, TE (TEA) CO_2 Doppler lidars can be used as typical aerosol lidars for sensing the planetary boundary layer.

The authors are grateful to R. Hardesty and R. Richter of NOAA for providing the NOAA ground-based Doppler lidar data. This research was supported in part by Bulgarian National Science Fund grant Ph-447.

References

1. R. M. Measures, *Laser Remote Sensing: Fundamentals and Applications* (Wiley, New York, 1984).
2. M. J. Kavaya and R. T. Menzies, "Lidar aerosol backscattering measurements: systematic, modeling, and calibration error consideration," Appl. Opt. **24,** 3444–3453 (1985).
3. L. L. Gurdev, D. V. Stoyanov, and T. N. Dreischuh, "Inverse algorithm for increasing the resolution of pulsed lidars," in *Coherent Laser Radar: Technology and Applications*, Vol. 12 of 1991 OSA Technical Digest Series (Optical Society of America, Washington, D.C., 1991), pp. 284–287.
4. L. L. Gurdev, T. N. Dreischuh, and D. V. Stoyanov, "Deconvolution techniques for improving the resolution of long-pulse lidars," J. Opt. Soc. Am. A **10,** 2296–2306 (1993).
5. T. N. Dreischuh, L. L. Gurdev, and D. V. Stoyanov, "On the influence of the pulse-shape uncertainty on the accuracy of Fourier-deconvolved lidar profiles," in *Proceedings of the 17th International Laser Radar Conference*, Sendai, Japan (Chiba University, Chiba, Japan, 1994), pp. 561–563.
6. T. N. Dreischuh, L. L. Gurdev, and D. V. Stoyanov, "Effect of pulse-shape uncertainty on the accuracy of deconvolved lidar profiles," J. Opt. Soc. Am. A **12,** 301–306 (1995).
7. R. Nordstrom, "A dual sensor role for pulsed CO_2 laser radar," Photonics Spectra **23,** 89–98 (1989).
8. Ch. Werner, G. Wildgruber, and J. Streicher, "Representativity of wind measurement from space," Final Report, European Space Agency Contract 8664/90/HGE-I, (German Aerospace Research Establishment, Munich, 1991).
9. J. Gilbert, J. L. Lachambre, F. Rheault, and R. Fortin, "Dynamics of the CO_2 atmospheric pressure excitation," Can. J. Phys. **50,** 2523–2535 (1972).